

Reentrant superconductivity in proximity to a topological insulator

T. Karabassov,¹ A. A. Golubov,^{2,3} V. M. Silkin,^{4,5,6} V. S. Stolyarov,^{3,7} and A. S. Vasenko^{1,8,*}

¹*HSE University, 101000 Moscow, Russia*

²*Faculty of Science and Technology and MESA⁺ Institute for Nanotechnology, University of Twente, 7500 AE Enschede, The Netherlands*

³*Moscow Institute of Physics and Technology, 141700 Dolgoprudny, Russia*

⁴*Donostia International Physics Center (DIPC), Paseo Manuel de Lardizabal 4, San Sebastián/Donostia, 20018 Basque Country, Spain*

⁵*Departamento de Física de Materiales, Facultad de Ciencias Químicas, UPV/EHU, 20080 San Sebastián, Basque Country, Spain*

⁶*IKERBASQUE, Basque Foundation for Science, 48011 Bilbao, Spain*

⁷*Dukhov Research Institute of Automatics (VNIIA), 127055 Moscow, Russia*

⁸*I.E. Tamm Department of Theoretical Physics, P.N. Lebedev Physical Institute, Russian Academy of Sciences, 119991 Moscow, Russia*

(Dated: February 14, 2022)

In the following paper we investigate the critical temperature T_c behavior in the two-dimensional S/TI (S denotes superconductor and TI - topological insulator) junction with a proximity induced in-plane helical magnetization in the TI surface. The calculations of T_c are performed using the general self-consistent approach based on the Usadel equations in Matsubara Green's functions technique. We show that the presence of the helical magnetization leads to the nonmonotonic behavior of the critical temperature as a function of the topological insulator layer thickness.

PACS numbers: 74.25.F-, 74.45.+c, 74.78.Fk

I. INTRODUCTION

Topological state of matter has been receiving a lot of attention for the past decade.^{1–5} Particularly, three-dimensional topological insulators (3D TI) have large potential for fault tolerant quantum computation.^{6,7} This is possible due to strong spin-orbit coupling (SOC) and time reversal symmetry that take place in such materials. There are special topologically protected states on the surface of the 3D topological insulator. These surface states are Dirac helical states, i.e., their spin and momentum are coupled in a well defined way resulting in a spin-momentum locking effect. Interesting transport properties are revealed when topological insulator and superconductor are in proximity to each other, forming a hybrid structure.⁸ In such hybrids in the presence of a magnetic field or a magnetic moment of an adjacent ferromagnet, zero energy Majorana modes can arise.^{9–14}

The proximity effect^{15–20} that takes place in superconducting hybrid structures can lead to various phenomena occurring near interfaces. For instance, critical temperature T_c behaves nonmonotonically as a function of different system parameters in S/F bilayers with uniform magnetization²¹ and multilayered S/F spin-valves with a magnetization misalignment in F layers²². Particularly, T_c demonstrates reentrant behavior under certain range of parameters.²¹ Such behavior originates from nontrivial dependence of Cooper pair wavefunction, which can also result in oscillating Josephson critical current^{23–29}, density of states^{30,31} and critical temperature^{32–36} in S/F/S junctions.

According to the theory developed in Refs. 10 and 37, there are no Josephson critical current oscillations in hy-

brid S/TI/S structures with a proximity induced uniform in-plane field in the TI layer. At the same time, as predicted in Ref. 37, the critical current demonstrates oscillatory behavior in case when the TI surface with helical magnetization serves as a weak link. Following the results of Zuyzin *et al.*³⁷, the observation of $0 - \pi$ phase transitions in the critical supercurrent may imply nontrivial critical temperature behavior and in particular the reentrant T_c behavior in the S/TI junction. Therefore, investigation of the T_c in the hybrids with both spin-orbit coupling and helical magnetization is essential for further understanding of the underlying physics and potential future applications. As far as we know, the critical temperature in S/TI structures has not been studied yet.

Spin-orbit effects have been discussed actively in the framework of the quasiclassical Green's functions approach in layered structures.^{17,18,38–45} Recently, the generalized quasiclassical theory was developed for a two-dimensional system with SOC and an exchange field both much greater than the disorder strength.⁴⁶ It has been shown that spontaneous supercurrent can flow in a Josephson junction, where magnetized superconductors are weakly coupled through the surface of 3D TI.⁴⁷

The goal of this work is to provide a quantitative investigation of the critical temperature in the S/TI hybrid structure as a function of its parameters applying the quasiclassical Green's function approach. The helical magnetization pattern considered in this paper is similar to one previously studied in S/F bilayers with nonuniform spiral magnets.^{48–50} Particularly, the superconducting spin valve consisting of a superconducting layer and a spiral magnetic was proposed for the spintronic application, using re-orientation of the spiral direction as a

method of the spin-valve control.^{51–53} However, nature of the effects that appear in our structure is different, since they are caused not only by in-plane helical magnetization pattern, but also by the spin-orbit coupling.

The paper is organized as follows. In Sec. II, we formulate the theoretical model and basic equations for the cases of $h(y)$ and $h(x)$ helical magnetizations. In Sec. III we present the results of the critical temperature calculations using the single-mode approximation. The results are concluded in Sec. IV.

II. MODEL

In this work we consider the 2D nanostructure, which is depicted in the Fig. 1. It consists of superconductor S of thickness d_s and topological insulator (TI) of thickness d_n with a proximity induced helical magnetization pattern of the following types:

$$\mathbf{h}(y) = h_0(\cos Qy, \sin Qy, 0), \quad (1)$$

$$\mathbf{h}(x) = h_0(\cos Qx, \sin Qx, 0), \quad (2)$$

where $Q = 2\pi/\lambda$ and λ determines the actual pattern of helical magnetization. It is important to note that we consider the variations of the magnetization \mathbf{h} in the x - y plane. Similar helical pattern with a period $\lambda \approx 10\text{nm}$ was observed experimentally in manganese on a tungsten substrate.⁵⁴ The orientation of the structure is along the x direction. In order to observe the inverse proximity effect the superconductor must be two-dimensional. Such disordered homogeneous superconducting 2D films can be obtained with the help of modern deposition techniques⁵⁵.

To calculate the critical temperature $T_c(d_n)$ of this structure we assume the diffusive limit, when the elastic scattering length ℓ is much smaller than the coherence length, and use the framework of the linearized Usadel equations for the S and TI layers in Matsubara representation.^{56,57} We perform the calculations in the low proximity limit expanding the Green's function around the bulk solution,

$$\hat{g} = \begin{pmatrix} \text{sgn } \omega_n & f \\ -\bar{f} & -\text{sgn } \omega_n \end{pmatrix} \quad (3)$$

Such limit is experimentally feasible and can be easily achieved in the vicinity of the superconducting critical temperature T_c or in a hybrid structures with low transparent interfaces.

A. Helical magnetization $\mathbf{h}(\mathbf{y})$

In this subsection we establish the equations for the magnetization pattern evolving along the S/TI interface indicated in Eq. (1), i. e. in y direction. Since the low proximity limit is assumed, near T_c the normal Green's function in a superconductor is $g_s = \text{sgn } \omega_n$, and the

Usadel equation for the anomalous Green's function f_s take the following form. In the S layers ($0 < x < d_s$) it reads

$$\xi_s^2 \pi T_{cs} \left(\frac{\partial^2}{\partial x^2} + \frac{\partial^2}{\partial y^2} \right) f_s - |\omega_n| f_s + \Delta = 0. \quad (4)$$

In the TI layer we consider the Usadel equation derived in Ref. 37,

$$\left(\frac{\partial}{\partial x} - \frac{2i}{\alpha} h_y(y) \right)^2 f_T + \left(\frac{\partial}{\partial y} + \frac{2i}{\alpha} h_x(y) \right)^2 f_T = \frac{|\omega_n|}{\xi_n^2 \pi T_{cs}} f_T \quad (5)$$

Since we consider the dirty limit, the spinless Green's function matrix \hat{g}_s is used in our calculations, whereas the spin texture is contained in the matrix $\check{g}(\mathbf{n}_F) = \hat{g}(1 + \hat{\eta} \cdot \mathbf{n}_F)/2$, where $\mathbf{n}_F = \mathbf{p}_F/p_F$ and $\hat{\eta} = (-\sigma_2, \sigma_1)$. The spin-momentum locking effect can be seen from the spin matrix \check{g} , so that spin and momentum are always fixed at the right angle.

Finally, the self-consistency equation reads,⁵⁶

$$\Delta \ln \frac{T_{cs}}{T} = \pi T \sum_{\omega_n} \left(\frac{\Delta}{|\omega_n|} - f_s \right). \quad (6)$$

In Eqs. (4)-(6) $\xi_s = \sqrt{D_s/2\pi T_{cs}}$, $\xi_n = \sqrt{D_n/2\pi T_{cs}}$, $\omega_n = 2\pi T(n + \frac{1}{2})$, where $n = 0, \pm 1, \pm 2, \dots$ are the Matsubara frequencies, T_{cs} is the critical temperature of the superconductor S, and $f_{s(T)}$ denotes the singlet components of anomalous Green function in the S(TI) region (we assume $\hbar = k_B = 1$).

As far as our 2D system is periodic in y direction and large values of helical magnetization parameter Q are considered such that $\lambda \ll W_f$, we can expand the anomalous Green functions using the Fourier series. The function f_T then can be written as,

$$f_T(x, y) = \sum_{p=-\infty}^{+\infty} f_T^{(p)}(x) e^{ipQy}. \quad (7)$$

The Usadel equation in the TI layer for the amplitudes $f_T^{(p)}$ then takes the following form,

$$\left(\frac{\partial}{\partial x} - \frac{2i}{\alpha} h_y(y) \right)^2 f_T^{(p)} - p^2 Q^2 f_T^{(p)} - \frac{4pQ h_x(y)}{\alpha} f_T^{(p)} = \left(\frac{|\omega_n|}{\xi_n^2 \pi T_{cs}} + \frac{4h_x^2(y)}{\alpha^2} - \frac{2ih'_x(y)}{\alpha} \right) f_T^{(p)}, \quad (8)$$

where, $h'_x(y)$ is a derivative of h_x along the y direction. Whereas, in the S layer the singlet function f_s as well as Δ can also be expanded into a Fourier series,

$$f_s(x, y) = \sum_{p=-\infty}^{+\infty} f_s^{(p)}(x) e^{ipQy}, \quad (9)$$

$$\Delta(x, y) = \sum_{p=-\infty}^{+\infty} \Delta^{(p)}(x) e^{ipQy}. \quad (10)$$

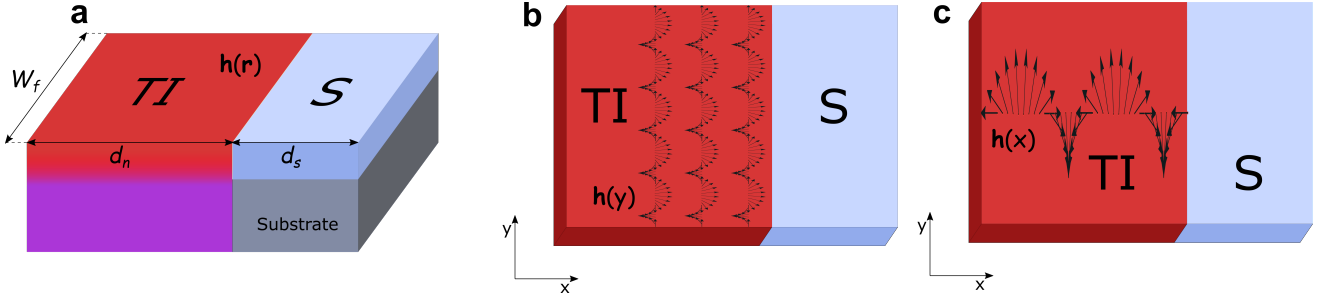


FIG. 1. (Color online) (a) Schematic of a 3D topological insulator (TI) - superconductor (S) junction with a proximity induced helical magnetization pattern. The magnetization vector is given by $\mathbf{h}(y) = h_0(\cos Qy, \sin Qy, 0)$ (b) and $\mathbf{h}(x) = h_0(\cos Qx, \sin Qx, 0)$ (c). The junction resides in the x - y plane and the S/TI interface lie in the y direction at $x = 0$. d_n and d_s are the thicknesses of TI and S layers respectively, while W_f is the width of the junction. γ_B is a transparency parameter which is proportional to the interface resistance.

The amplitudes $f_s^{(p)}$ obey the following equation,

$$\xi_s^2 \left(\frac{\partial^2 f_s^{(p)}}{\partial x^2} - p^2 Q^2 f_s^{(p)} - \frac{|\omega_n|}{\xi_s^2 \pi T_{cs}} f_s^{(p)} \right) + \frac{\Delta^{(p)}}{\pi T_{cs}} = 0. \quad (11)$$

The self-consistency equation for the Fourier amplitudes in the superconductor can be written as,

$$\Delta^{(p)} \ln \frac{T_{cs}}{T} = \pi T \sum_{\omega_n} \left(\frac{\Delta^{(p)}}{|\omega_n|} - f_s^{(p)} \right). \quad (12)$$

From the equations above, it is clear that the amplitudes of the Fourier series are decoupled in the vicinity of the critical temperature. Therefore, each Fourier component p satisfies certain Usadel equation and the boundary conditions. Moreover, every single Fourier harmonic p of anomalous Green function $f_s^{(p)}$ and pair amplitude $\Delta^{(p)}$ determines particular T_c through the corresponding gap equation. However, the physical solution is the one, which gives the highest critical temperature T_c , i. e. the solution is energetically favorable.

We also need to supplement the equations above with proper boundary conditions to solve the problem.^{37,58} We assume low transparency limit of the interface between topological insulator (TI) and superconducting layer (S). It is also assumed that spin is conserved when the electrons tunnel across the interface, whereas momentum is not conserved. For the Fourier harmonics of the solution $f^{(p)}$ that we have introduced above taking all the simple transformations into account, the boundary conditions at $x = 0$ take the form,

$$\gamma_B \xi_n \left(\frac{\partial}{\partial x} - \frac{2ih_y(y)}{\alpha} \right) f_T(0) = f_s(0) - f_T(0), \quad (13)$$

$$\gamma \xi_n \left(\frac{\partial}{\partial x} - \frac{2ih_y(y)}{\alpha} \right) f_T(0) = \xi_s \frac{\partial f_s(0)}{\partial x}. \quad (14)$$

Here we omitted the component index p . The parameter $\gamma_B = R_b \sigma_n / \xi_n$ is transparency parameter which is

the ratio of resistance per unit area of the surface of the tunneling barrier to the resistivity of the TI layer and describes the effect of the interface barrier^{58,59}. In (14) the dimensionless parameter $\gamma = \xi_s \sigma_n / \xi_n \sigma_s$ determines the strength of suppression of superconductivity in the S layers near the S/TI interface compared to the bulk (inverse proximity effect). No suppression occurs for $\gamma = 0$, while strong suppression takes place for $\gamma \ll 1$. Here $\sigma_{s(n)}$ is the normal-state conductivity of the S(TI) layer. These boundary conditions should also be supplemented with vacuum conditions at the edges ($x = -d_n$ and $x = +d_s$),

$$\frac{\partial f_s(d_s)}{\partial x} = 0, \quad \left(\frac{\partial}{\partial x} - \frac{2ih_y(y)}{\alpha} \right) f_T(-d_n) = 0. \quad (15)$$

The solution of the equation (8) can be found in the form,

$$f_T^{(p)} = C(\omega_n) \cosh \kappa_{p,y} (x + d_n) \exp \left[i \frac{2h_y(y)}{\alpha} (x + d_n) \right], \quad (16)$$

where,

$$k_{p,y} = \sqrt{\frac{|\omega_n|}{\xi_n^2 \pi T_{cs}} + \frac{4}{\alpha^2} h_y^2(y) - \frac{2ih'_x(y)}{\alpha}} + Q_p, \\ Q_p = p^2 Q^2 + \frac{4pQh_x(y)}{\alpha}.$$

Here $C(\omega_n)$ is the coefficient, which is found from the boundary conditions and the wavevector acquires additional imaginary term due to fast oscillations of the anomalous Green's function along the y direction compared to the case of uniform magnetization ($Q = 0$). The introduced solution to the equation automatically satisfies the vacuum boundary conditions (15).

As far as Δ is assumed to be real valued function, we write our equations for anomalous Green's functions in real form. Also we consider only positive Matsubara frequencies ω_n . Following the standard procedure we obtain final set of equations which are sufficient to calculate critical temperature as a function of d_n .

Using the boundary conditions (13)-(14) we would like to write the problem in a closed form with respect to the Green's function f_s . At $x = 0$ the boundary conditions can be written as:

$$\xi_s \frac{\partial f_s(0)}{\partial x} = \frac{\gamma}{\gamma_b + A_{pT}(\omega_n)} f_s(0), \quad (17)$$

where

$$A_{pT}(\omega_n) = \frac{1}{k_{p,y}} \coth k_{p,y} d_n.$$

The boundary condition (17) is complex. In order to rewrite it in a real form, we use the following relation,

$$f^\pm = f(\omega_n) \pm f(-\omega_n). \quad (18)$$

According to the Usadel equation (4), there is a symmetry relation $f(-\omega_n) = f^*(\omega_n)$ which implies that f^+ is a real while f^- is a purely imaginary function. Then, we rewrite the Usadel equation in the S layer in terms of f_s^+ and f_s^- utilizing symmetry relation (18). Since the pair potential Δ is considered to be real valued function, we can find the solution analytically in the Usadel equation for the imaginary function f_s^- . Using the solution found analytically, it is possible to derive the complex boundary condition (17) in real form for the function f_s^+ ,

$$\xi_s \frac{\partial f_s^+(0)}{\partial x} = W^{(p)}(\omega_n) f_s^+(0), \quad (19)$$

where we used the notations,

$$W^{(p)}(\omega_n) = \gamma \frac{A_{ps}(\gamma_b + \text{Re } A_{pT}) + \gamma}{A_{ps}|\gamma_b + A_{pT}|^2 + \gamma(\gamma_b + \text{Re } A_{pT})}, \quad (20)$$

$$A_{ps} = \kappa_{ps} \tanh \kappa_{ps} d_s, \quad A_{pT}(\omega_n) = \frac{1}{k_{p,y}} \coth k_{p,y} d_n,$$

$$\kappa_{ps} = \sqrt{Q^2 p^2 + \frac{|\omega_n|}{\xi_s^2 \pi T_{cs}}}.$$

In the same way we rewrite the self-consistency equation for Δ in terms of symmetric function f_s^+ considering only positive Matsubara frequencies,

$$\Delta^{(p)} \ln \frac{T_{cs}}{T} = \pi T \sum_{\omega_n > 0} \left(\frac{2\Delta^{(p)}}{\omega_n} - f_s^{(p)+} \right), \quad (21)$$

as well as the Usadel equation in the superconducting S layer,

$$\xi_s^2 \left(\frac{\partial^2 f_s^{(p)+}}{\partial x^2} - \kappa_{ps}^2 f_s^{(p)+} \right) + \frac{2\Delta^{(p)}}{\pi T_{cs}} = 0. \quad (22)$$

To calculate the critical temperature in the system considered, we use the equations (19)-(22), together with the vacuum boundary condition (15) for the Fourier components $f_s^{(p)+}$.

B. Helical magnetization $\mathbf{h}(\mathbf{x})$

Here we consider the system consisting of a superconductor and topological insulator with helical magnetization pattern presented in the Eq. (2). In this case the Usadel equation should be rewritten in terms of magnetization $\mathbf{h}(x)$. We assume that the anomalous Green's function does not depend on y coordinate and thus the corresponding derivatives are neglected. The Usadel equation in the TI layer then takes the following form,

$$\left(\frac{\partial}{\partial x} - \frac{2ih_y(x)}{\alpha} \right)^2 f - \frac{4h_x^2(x)}{\alpha^2} f = \frac{|\omega_n|}{\xi_n^2 \pi T_{cs}} f \quad (23)$$

In order to rewrite the Eq. (23) in real form we introduce the following ansatz,

$$f(x) = f_L(x) \exp \left[-i \frac{2h_0}{\alpha Q} \cos Qx \right]. \quad (24)$$

Inserting this substitution into the Eq. (23), we obtain the equation for real valued function in the TI layer,

$$\frac{\partial^2 f_L}{\partial x^2} = \left(\frac{|\omega_n|}{\xi_n^2 \pi T_{cs}} + \frac{4h_0^2 \cos^2 Qx}{\alpha^2} \right) f_L \quad (25)$$

For this system we utilize the same boundary conditions as in previous subsection and express them in real form using symmetry relation (18). After the substitutions the boundary conditions take the form,

$$\gamma_B \xi_n \frac{\partial f_L(0)}{\partial x} = C_0 f_s^+(0) - f_L(0), \quad (26)$$

$$\gamma \xi_n \frac{\partial f_L(0)}{\partial x} = \xi_s C_0 \frac{\partial f_s^+(0)}{\partial x}. \quad (27)$$

where $C_0 = \cos(2h_0/\alpha Q)$. Finally, the boundary conditions at the free edges at $x = d_s$ and $x = -d_n$,

$$\frac{\partial f_s(d_s)}{\partial x} = 0, \quad \frac{\partial f_T(-d_n)}{\partial x} = 0. \quad (28)$$

Similarly, we introduce the self-consistency equation for Δ in terms of symmetric function f_s^+ treating only positive Matsubara frequencies,

$$\Delta \ln \frac{T_{cs}}{T} = \pi T \sum_{\omega_n > 0} \left(\frac{2\Delta}{\omega_n} - f_s^+ \right), \quad (29)$$

and the Usadel equation in the S layer,

$$\xi_s^2 \pi T_{cs} \frac{\partial^2 f_s^+}{\partial x^2} - \omega_n f_s^+ + 2\Delta = 0, \quad (30)$$

Since the Eq. (23) can not be solved analytically, to obtain the critical temperature T_c the whole set of equations (25)-(30) must be calculated numerically.

C. Single-mode approximation

In this subsection we present the single mode approximation method. The solution of the problems (19)-(22) and (25)-(30) can be searched in the form of the following ansatz,

$$f_s^+(x, \omega_n) = f(\omega_n) \cos\left(\Omega \frac{x - d_s}{\xi_s}\right), \quad (31a)$$

$$\Delta(x) = \delta \cos\left(\Omega \frac{x - d_s}{\xi_s}\right), \quad (31b)$$

where δ and Ω do not depend on ω_n . The above solution automatically satisfies boundary condition (15) at $x = d_s$.

1. Case of $\mathbf{h}(\mathbf{y})$

Substituting expression (31) into the (22) we obtain,

$$f(\omega_n) = \frac{2\delta}{\Omega^2 \pi T_{cs} + \pi T_{cs} \xi_s^2 Q^2 p^2}. \quad (32)$$

To determine the critical temperature T_c we have to substitute the Eqs. (31)-(32) into the self-consistency equation (21) at $T = T_c$. Then it is possible to rewrite the self-consistency equation in the following form,

$$\ln \frac{T_{cs}}{T_c} = \psi\left(\frac{1}{2} + \frac{\Omega^2 + Q^2 p^2 T_{cs}}{2 T_c}\right) - \psi\left(\frac{1}{2}\right), \quad (33)$$

where ψ is the digamma function,

$$\psi(z) \equiv \frac{d}{dz} \ln \Gamma(z), \quad \Gamma(z) = \int_0^\infty \eta^{z-1} e^{-\eta} d\eta. \quad (34)$$

Boundary condition (19) at $x = 0$ yields the following equation for Ω ,

$$\Omega \tan\left(\Omega \frac{d_s}{\xi_s}\right) = W^{(p)}(\omega_n). \quad (35)$$

Generally, in order to calculate the critical temperature T_c , the problem is put on the grid with finite number of the Fourier harmonics N and the following condition should be used,

$$T_c = \max\left(T_c^{(p)}\right) \quad p = 0, 1, 2 \dots N. \quad (36)$$

The critical temperature behavior is found from the solution of the transcendental equations (33), (35) as well as Eq. (36). Thus, the solution that gives the highest critical temperature T_c is the only one, which is realized physically.

However, we find that to calculate the critical temperature it is sufficient to use the zeroth ($p = 0$) harmonic of the full Fourier solution for the certain parameter range.

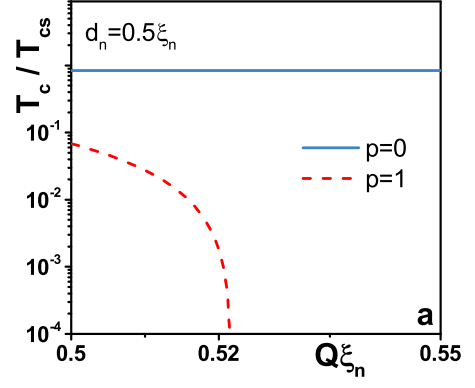


FIG. 2. (Color online). $T_c(Q)$ dependencies for two harmonic solutions at $\xi_n h_0 / \alpha = 0.1$. The behavior realized physically is the one which gives the highest T_c . The parameters used in the calculations: $\gamma_B = 0.1$, $W_f = 100 \xi_n$

In Fig. 2 we demonstrate the parameter regime, for which the T_c calculation requires consideration of only $p = 0$ Fourier component. Such situation is possible due to rapid decay of the $p > 0$ components of the solution as functions of Q . From the plot it can be noticed that for $Q \xi_n > 0.5$ the critical temperature for $p = 1$ is not only lower than T_c for $p = 0$ but rapidly drops to zero at $Q \xi_n \approx 0.52$.

Such behaviour of the $p > 0$ components allows us to operate in the parameter regime by taking appropriate $Q \gg 1$, where the $p = 0$ harmonic is sufficient for description of the T_c in the bilayer. Since the function oscillates quickly ($Q \xi_n \gg 1$), we also perform averaging of the critical temperature T_c along the y direction.

2. Case of $\mathbf{h}(\mathbf{x})$

As far as the solution of the Eq. (25) can not be found in analytical form, we calculate the function f_L numerically and solve the problem (25)-(30) incorporating single mode approximation (31).

III. RESULTS AND DISCUSSION

In this section we present the results of the critical temperature calculations using the single-mode approximation. Some of the parameters are set to the certain values and are not changed throughout the paper, otherwise it is indicated. Such parameters are: $\gamma = 0.2$, $\xi_s = \xi_n$ and the width of the junction $W_f = 20 \xi_n$.

A. Case of $\mathbf{h}(\mathbf{y})$

In Fig. 3 (a) the critical temperature dependencies are plotted for different values of the transparency parameter γ_B . The helical magnetization parameter $\xi_n h_0 / \alpha = 0.25$

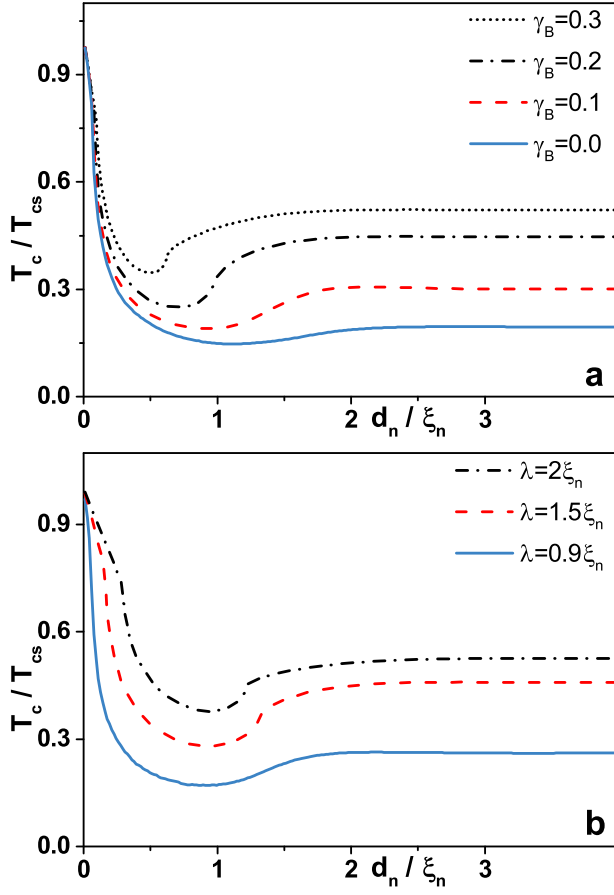


FIG. 3. (Color online). Behavior of the critical temperature T_c as a function of d_n . (a) Each plot corresponds to particular value of the transparency parameter γ_B : blue solid line to $\gamma_B = 0$, red dashed line to $\gamma_B = 0.1$, black dash-dotted line to $\gamma_B = 0.2$ and dotted line to $\gamma_B = 0.3$. (b) Effect of λ on $T_c(d_n)$ dependence. Each curve corresponds to particular value of λ : blue solid line to $\lambda = 0.9\xi_n$, red dashed line to $\lambda = 1.5\xi_n$ and black dash-dotted line to $\lambda = 2\xi_n$. The parameters used in the calculations: $\xi_n h_0/\alpha = 0.25$, $Q = 2\pi/\lambda$, $\lambda = \xi_n$ (for plot a), $d_s = 1.2\xi_s$.

and $\lambda = \xi_n$ ($\lambda = 2\pi/Q$). We normalize T_c by its maximum value T_{cs} in the absence of the proximitized TI layer and the TI thickness d_n by the coherence length ξ_n . As expected, for perfectly transparent S/TI interface (blue solid line) the critical temperature decreases significantly, showing nonmonotonic behavior with a minimum at $d_n \approx \xi_n$ and eventually saturates at $T_c \approx 0.15T_{cs}$. For larger values of γ_B or at moderate and high resistances of the interface $T_c(d_n)$ saturates at larger temperatures and what is more interesting, the position of the T_c minimum shifts towards smaller values of d_n . Unlike $T_c(d_n)$ dependencies in ordinary S/F systems with uniform as well as out of plane spiral magnetization, here the critical temperature does not demonstrate completely reentrant behavior, i. e. the T_c does not vanish in a certain interval of d_n . The impact of different λ on the critical temperature behavior is depicted in Fig. 3 (b). Here we

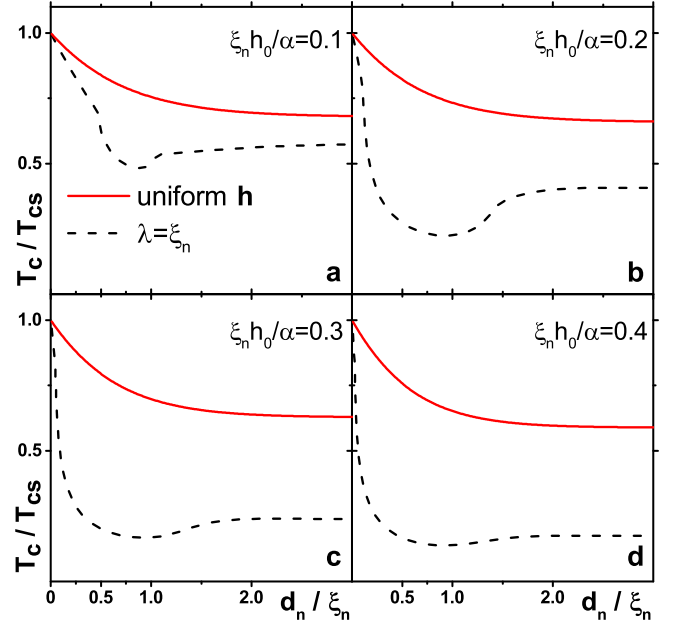


FIG. 4. (Color online). Comparison of the critical temperature behavior between the S/TI bilayer with uniform magnetization and S/TI bilayer with helical magnetization pattern introduced in Eq. (1). The curves were calculated for different values of the h_0/α : plot (a) corresponds to $\xi_n h_0/\alpha = 0.1$, plot (b) to $\xi_n h_0/\alpha = 0.2$, plot (c) to $\xi_n h_0/\alpha = 0.3$ and plot (d) to $\xi_n h_0/\alpha = 0.4$. The general parameters in the bilayers have been set to the identical values such as γ and the coherence lengths. The transparency parameter is also same for the both systems $\gamma_B = 0.1$.

took $\gamma_B = 0.1$, $\xi_n h_0/\alpha = 0.25$ and $d_s = 1.2\xi_s$. From the graph one can notice that T_c becomes more suppressed for smaller values of spatial period λ (which is expressed in terms of Q as $\lambda = 2\pi/Q$), which means that λ acts as an additional cause of the superconducting correlations depairing. It is worth mentioning that rather opposite effect has been observed in the S/F hybrid bilayers with out of plane spiral magnetization⁴⁹, where T_c experienced enhancement as Q increased.

B. Uniform and helical magnetization

In this subsection we compare the $T_c(d_n)$ behavior in S/TI bilayers with the uniform and helical magnetisation induced on the TI surface. In Fig. 4 the comparison between S/TI with uniform \mathbf{h} and with $\mathbf{h}(y)$ is shown. From the figure one can see that there is a significant difference in the $T_c(d_n)$ dependence for both cases. First, let us discuss the origin of T_c suppression in the case of uniformly magnetized TI surface. The wavevector of the pair correlations in topological insulator can be written as,

$$\kappa_0 = \sqrt{\frac{2\omega_n}{D} + \frac{4}{\alpha^2}h_x^2}, \quad (37)$$

where h_x is the magnetization component along the x direction. Here h_x is responsible for depairing of the superconducting correlations and suppresses the critical temperature T_c with the decay length $\xi = 1/\kappa \approx \min[\sqrt{2\omega_n/D}, \alpha/2h_x]$. However, h_y component of the magnetization does not play role in suppression of superconducting correlations but introduces a phase shift in the wavefunction, which has no quantitative effect on T_c .

Thus, in Fig. 4 the critical temperature in case of uniform magnetization (red solid lines) expresses monotonic decay due to h_x component. Other type of behavior appears when large enough values of Q are considered in the system. In this case the wavevector acquires additional imaginary term of the form (16) and decay length squared now becomes inverse proportional to Q as $\xi = 1/\kappa \approx \min[\sqrt{2\omega_n/D}, \alpha/2h_0, \sqrt{\alpha/2h_0Q}]$. In fact, T_c demonstrates nonmonotonic behavior due to fast oscillations of helical magnetization along y axis. This behavior is indicated by black dashed lines (Fig. 4) and it can be seen that $T_c(d_n)$ loses its nonmonotonicity as h_0/ξ_n grows from clearly pronounced (plots a and b) to hardly recognizable minimum (plots c and d) in the dependence.

C. Case of $\mathbf{h}(\mathbf{x})$

Now we turn to the case of S/TI hybrid structure with the TI layer magnetized along the x -axis [Fig. 1 (c)]. In Fig. 5 the critical temperature dependencies as functions of the TI layer thickness d_n are shown. The effect of varying magnetization strength h_0 with parameter Q fixed to $Q = 2.0$ is shown in the upper plot [Fig. 5 (a)]. From the plot we can distinguish three types of T_c behavior. For small values of h_0/α the critical temperature demonstrates slightly nonmonotonic behavior with a kink at around $d_n \approx \xi_n$ and eventual saturation (a black dotted line). This nonmonotonic feature becomes more pronounced as h_0/α is increased (a blue solid line). However, for certain value of magnetization strength h_0 the critical temperature drops to zero gradually (a red dashed line). Finally, at relatively large h_0 the critical temperature drops sharply down to zero without any bend (a black dash-dotted line).

The origin of such $T_c(d_n)$ curves is a coupling of helical magnetization and momentum of the quasiparticles. However, unlike the magnetization pattern $h(y)$, here the topological insulator TI is magnetized by $h(x)$ along the direction of d_n . Hence, the effects on the critical temperature are more explicit and clearer to understand. As it was discussed above, h_y component has no quantitative impact on the magnitude of T_c , therefore, the observed effects are purely due to variation of h_x and namely because of its periodicity. Obviously, the number of kinks demonstrated in the Fig. 5(a), where we observed just one, depends on magnetization parameter $Q = 2\pi/\lambda$. In Fig. 5(b) the critical temperature behavior for different Q is shown. It can be seen that the smaller spatial magne-

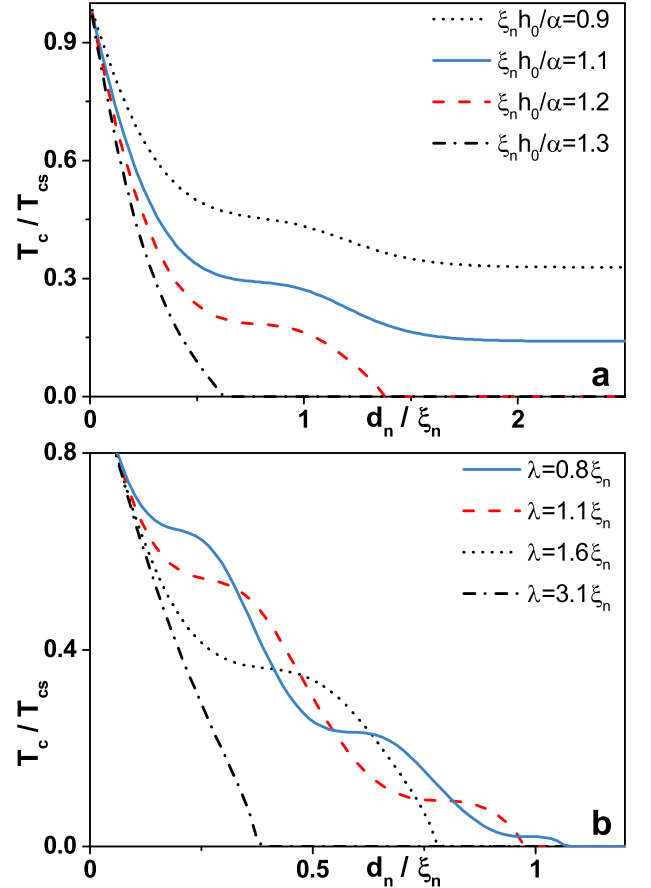


FIG. 5. (Color online). $T_c(d_n)$ dependencies for the configuration of helical magnetization introduced in Eq. (2). (a) Each curve corresponds to particular value of h_0/α with fixed helical magnetization parameter $Q = 2$. Black dotted line corresponds to $\xi_n h_0/\alpha = 0.9$, blue solid line to $\xi_n h_0/\alpha = 1.1$, red dashed line to $\xi_n h_0/\alpha = 1.2$ and black dash-dotted line to $\xi_n h_0/\alpha = 1.3$ (b) The dependencies correspond to certain values of λ and fixed $\xi_n h_0/\alpha = 1.4$. Blue solid line - $\lambda = 0.8\xi_n$, red dashed line - $\lambda = 1.1\xi_n$, black dotted line - $\lambda = 1.6\xi_n$ and dash-dotted line - $\lambda = 3.1\xi_n$. The rest of the parameters used in the calculations: $\gamma_B = 0$, $d_s = 1.2\xi_s$

tization period λ the more kinks are produced in the T_c . In the calculations above we assumed that the magnetization pattern $\mathbf{h}(x)$ at $x = 0$ reduces to $\mathbf{h}(0) = h_0(1, 0, 0)$, which implies that the initial ‘phase’ is 0. In practice, it may be possible to have arbitrary initial phase in the experimental samples. It is very important to consider such possibility since T_c decays significantly in our system as a function of the TI thickness d_n . We can take into account ϕ_0 simply by rewriting the magnetization pattern (2) as,

$$\mathbf{h}(x) = h_0(\cos(Qx + \phi_0), \sin(Qx + \phi_0), 0). \quad (38)$$

In Fig. 6 (a) the effect of various initial ϕ_0 on $T_c(d_n)$ for fixed $h_0/\alpha = 1.4$ and $\lambda = \xi_n$ is illustrated. From the plot we observe that while $\phi_0 = 0$ and $\phi_0 = \pi/4$ contribute to faster decay of T_c as a function of d_n (red dotted and blue

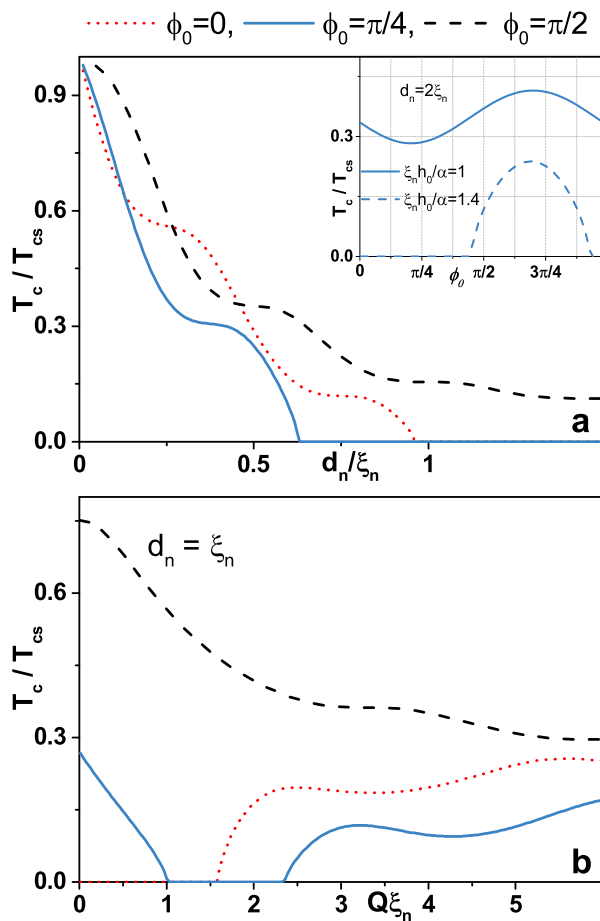


FIG. 6. (Color online). Influence of the arbitrary initial phase ϕ_0 in the magnetization pattern $\mathbf{h}(x) = h_0(\cos(Qx + \phi_0), \sin(Qx + \phi_0), 0)$. Each curve corresponds to particular value of ϕ_0 : red dotted line to $\phi_0 = 0$, blue solid line to $\phi_0 = \pi/4$ and black dashed line to $\phi_0 = \pi/2$. (a) $T_c(d_n)$ dependencies calculated for $\xi_n h_0/\alpha = 1.4$ and $\lambda = \xi_n$. The inset plot shows T_c behavior as a function of phase ϕ_0 for fixed thickness $d_n = 2\xi_n$ and two different values of $\xi_n h_0/\alpha = 1, 1.4$. (b) $T_c(Q)$ curves calculated for $d_n = \xi_n$ and $\xi_n h_0/\alpha = 1.2$. The parameters used in the calculations: $\gamma_B = 0$, $\xi_n h_0/\alpha = 0.25$ and $d_s = 1.2\xi_s$.

solid line), the critical temperature has higher values at almost every d_n for $\phi_0 = \pi/2$ (black dashed line). The inset shows T_c as a function of ϕ_0 for fixed $d_n = 2\xi_n$.

Another interesting result can be noticed in Fig. 6 (b) illustrating $T_c(Q)$ dependencies for the same values of ϕ_0 and fixed TI layer thickness $d_n = \xi_n$. One can recognize

that depending on ϕ_0 the critical temperature behaves differently as Q changes. For $\phi_0 = 0$ (red dotted line) there is no superconductivity in the $Q\xi_n$ interval $[0, 1.5]$ since T_c is completely suppressed by slowly evolving near extremum h_x magnetization component at the vicinity of the S/TI interface. However, for $\phi_0 = \pi/4$ (blue solid line) T_c decays rapidly and vanishes at $Q\xi_n \approx 1$ but eventually restores at $Q\xi_n \approx 2.4$. Finally in the case of $\phi_0 = \pi/2$ (black dashed line) the critical temperature is almost not suppressed at small values of Q , but decays gradually as Q is further increased.

IV. CONCLUSION

In this work we have formulated a theoretical approach and presented the results of a quantitative investigation of the superconducting critical temperature in the S/TI hybrid structure, where an in-plane helical magnetization is induced at the TI surface. The calculations are based on the quasiclassical Usadel equations, taking into account SOC at the surface of the topological insulator. We have found that in the case of in-plane helical magnetization $\mathbf{h}(y)$, evolving along the interface, the calculations reveal nonmonotonic behavior of the critical temperature as a function of the TI layer thickness with a well pronounced minimum, the effect which is absent in the case of uniform magnetization. Moreover, in the case of helical magnetization, evolving perpendicular to the interface $\mathbf{h}(x)$, the critical temperature demonstrates highly nonmonotonic behavior as well. However, this dependence has been shown to be qualitatively different from the case of $\mathbf{h}(y)$, showing number of kinks, which depends on helical magnetization parameters.

The results are important for further understanding of the underlying physics and potential future applications of superconductor - TI hybrid systems.

ACKNOWLEDGMENTS

T.K. and A.S.V. acknowledge support of the Mirror Laboratories project of the HSE University and the Bashkir State Pedagogical University. V.S.S. acknowledges support of the joint French (ANR) / Russian (RSF) Grant “CrysTop” (20-42-09033). A.A.G. acknowledges support by the European Union H2020-WIDESPREAD-05-2017-Twinning project SPINTECH under Grant Agreement No. 810144.

* avasenko@hse.ru

¹ L. Fu, C. L. Kane and E. J. Mele Phys. Rev. Lett. **98**, 106803 (2007).

² M. Z. Hasan and C. L. Kane, Rev. Mod. Phys., **82**, 3045 (2010).

³ M. Sato and Y. Ando, Reports on Progress in Physics **80**, 076501 (2017).

⁴ S.-Q. Shen, *Topological Insulators Dirac Equation in Condensed Matters* (Berlin: Springer, 2012).

⁵ G. Tkachov *Topological Insulators: The Physics of Spin*

- Helicity in Quantum Transport* (Singapore: Pan Stanford, 2015).
- ⁶ S. D. Sarma, M. Freedman and C. Nayak, *Phys. Today* **59**, 32 (2006).
 - ⁷ R. Aguado and L. P. Kouwenhoven, *Phys. Today* **73**, 44 (2020).
 - ⁸ X.-L. Qi and S.-C. Zhang, *Rev. Mod. Phys.* **83**, 1057 (2011).
 - ⁹ L. Fu, and C. L. Kane, *Phys. Rev. Lett.* **100**, 096407 (2008).
 - ¹⁰ Y. Tanaka, T. Yokoyama, and N. Nagaosa, *Phys. Rev. Lett.* **103**, 107002 (2009).
 - ¹¹ M. Sato and S. Fujimoto, *Phys. Rev. B* **79**, 094504 (2009).
 - ¹² J. Alicea, *Rep. Prog. Phys.* **75**, 076501 (2012).
 - ¹³ C. W. J. Beenakker, *Annu. Rev. Condens. Matter Phys.* **4**, 113 (2013).
 - ¹⁴ G. Tkachov and E. N. Hankiewicz, *Phys. Rev. B* **88**, 075401 (2013).
 - ¹⁵ E. A. Demler, G. B. Arnold, and M. R. Beasley, *Phys. Rev. B* **55**, 15174 (1997).
 - ¹⁶ A. Ozaeta, A. S. Vasenko, F. W. J. Hekking, and F. S. Bergeret, *Phys. Rev. B* **86**, 060509(R) (2012).
 - ¹⁷ F. S. Bergeret and I. V. Tokatly, *Phys. Rev. Lett.* **110**, 117003 (2013).
 - ¹⁸ I. V. Bobkova and A. M. Bobkov, *Phys. Rev. B* **95**, 184518 (2017).
 - ¹⁹ F. S. Bergeret, A. F. Volkov, and K. B. Efetov, *Rev. Mod. Phys.* **77**, 1321 (2005).
 - ²⁰ A. I. Buzdin, *Rev. Mod. Phys.* **77**, 935 (2005).
 - ²¹ Y. V. Fominov, N. M. Chitchev, and A. A. Golubov, *Phys. Rev. B* **66**, 014507 (2002).
 - ²² Ya. V. Fominov, A. A. Golubov, T. Yu. Karminskaya, M. Yu. Kupriyanov, R. G. Deminov, L. R. Tagirov, *JETP Lett.* **91**, 308 (2010) [*Pis'ma ZhETF* **91**, 329 (2010)].
 - ²³ A. I. Buzdin, L. N. Bulaevskii, and S. V. Panyukov, *JETP Lett.* **35**, 178 (1982) [*Pis'ma ZhETF* **35**, 147 (1982)].
 - ²⁴ A. I. Buzdin and M. Yu. Kupriyanov, *JETP Lett.* **53**, 321 (1991) [*Pis'ma ZhETF* **53**, 308 (1991)].
 - ²⁵ V. V. Ryazanov, V. A. Oboznov, A. Yu. Rusanov, A. V. Veretennikov, A. A. Golubov, and J. Aarts, *Phys. Rev. Lett.* **86**, 2427 (2001).
 - ²⁶ V. A. Oboznov, V. V. Bol'ginov, A. K. Feofanov, V. V. Ryazanov, and A. I. Buzdin, *Phys. Rev. Lett.* **96**, 197003 (2006).
 - ²⁷ A. V. Vedyayev, N. V. Ryzhanova, N. G. Pugach, *Journal of Magnetism and Magnetic Materials*, **305**, 53 (2006).
 - ²⁸ A. S. Vasenko, A. A. Golubov, M. Yu. Kupriyanov, and M. Weides, *Phys. Rev. B* **77**, 134507 (2008).
 - ²⁹ S. V. Bakurskiy, V. I. Filippov, V. I. Ruzhickiy, N. V. Klenov, I. I. Soloviev, M. Yu. Kupriyanov, A. A. Golubov, *Phys. Rev. B* **95**, 094522 (2017).
 - ³⁰ T. Kontos, M. Aprili, J. Lesueur, and X. Gison, *Phys. Rev. Lett.* **86**, 304 (2001).
 - ³¹ A. S. Vasenko, S. Kawabata, A. A. Golubov, M. Yu. Kupriyanov, C. Lacroix, F. S. Bergeret, and F. W. J. Hekking, *Phys. Rev. B* **84**, 024524 (2011).
 - ³² J. S. Jiang, D. Davidović, D. H. Reich, and C. L. Chien, *Phys. Rev. Lett.* **74**, 314 (1995).
 - ³³ L. R. Tagirov, *Physica C* **307**, 145 (1998).
 - ³⁴ Yu. N. Proshin, Yu. A. Izyumov, and M. G. Khusainov, *Phys. Rev. B* **64**, 064522 (2001).
 - ³⁵ Yu. N. Khaydukov, A. S. Vasenko, E. A. Kravtsov, V. V. Progladio, V. D. Zhaketov, A. Csik, Yu. V. Nikitenko, A. V. Petrenko, T. Keller, A. A. Golubov, M. Yu. Kupriyanov, V. V. Ustinov, V. L. Aksenov, and B. Keimer, *Phys. Rev. B* **97**, 144511 (2018).
 - ³⁶ T. Karabassov, V. S. Stolyarov, A. A. Golubov, V. M. Silkin, V. M. Bayazitov, B. G. Lvov, and A. S. Vasenko, *Phys. Rev. B* **100**, 104502 (2019).
 - ³⁷ A. Zyuzin, M. Alidoust, and D. Loss, *Phys. Rev. B* **93**, 214502 (2016).
 - ³⁸ F.S. Bergeret and I. V. Tokatly, *Phys. Rev. B* **89**, 134517 (2014).
 - ³⁹ S. H. Jacobsen and J. Linder, *Phys. Rev. B* **92**, 024501 (2015).
 - ⁴⁰ B. Bujnowski, R. Biele, and F.S. Bergeret, *Phys. Rev. B* **100**, 224518 (2019).
 - ⁴¹ J. R. Eskilt, M. Amundsen, N. Banerjee, and Jacob Linder, *Phys. Rev. B* **100**, 224519 (2019).
 - ⁴² M. Nashaat, I. V. Bobkova, A.M. Bobkov, Y.M. Shukrinov, I.R. Rahmonov, and K. Sengupta, (2019).
 - ⁴³ I. V. Bobkova, A. M. Bobkov, A. A. Zyuzin, and M. Alidoust, *Phys. Rev. B* **94**, 134506 (2016).
 - ⁴⁴ M. Alidoust, *Phys. Rev. B* **98**, 245418 (2018).
 - ⁴⁵ M. Alidoust, *Phys. Rev. B* **101**, 155123 (2020).
 - ⁴⁶ Y. Lu and T.T. Heikkilä, *Phys. Rev. B* **100**, 104514 (2019).
 - ⁴⁷ M. Alidoust and H. Hamzehpour, *Phys. Rev. B* **96**, 165422 (2017).
 - ⁴⁸ T. Champel and M. Eschrig, *Phys. Rev. B* **71**, R220506 (2005).
 - ⁴⁹ T. Champel and M. Eschrig, *Phys. Rev. B* **72**, 054523 (2005).
 - ⁵⁰ T. Champel, T. Löfwander, and M. Eschrig, *Phys. Rev. Lett.* **100**, 077003 (2008).
 - ⁵¹ N.G. Pugach, M. Safonchik, T. Champel, M.E. Zhitomirsky, E. Lähderanta, M. Eschrig, and C. Lacroix, *Appl. Phys. Lett.* **111**, 162601 (2017).
 - ⁵² N.G. Pugach and M.O. Safonchik, *JETP Lett.* **107**, 302 (2018).
 - ⁵³ N.G. Pugach, M.O. Safonchik, D.M. Heim, and V.O. Yagovtsev, *Phys. Solid State* **60**, 2237 (2018).
 - ⁵⁴ M. Bode, M. Heide, K. Von Bergmann, P. Ferriani, S. Heinze, G. Bihlmayer, A. Kubetzka, O. Pietzsch, S. Blügel, and R. Wiesendanger, *Nature* **447**, 190 (2007).
 - ⁵⁵ C. Brun, T. Cren, and D. Roditchev, *Supercond. Sci. Technol.* **30** 013003 (2017).
 - ⁵⁶ W. Belzig, F. K. Wilhelm, C. Bruder, G. Schön, and A. D. Zaikin, *Superlattices Microstruct.* **25**, 1251 (1999).
 - ⁵⁷ K. D. Usadel, *Phys. Rev. Lett.* **25**, 507 (1970).
 - ⁵⁸ M. Yu. Kupriyanov and V. F. Lukichev, *JETP* **67**, 1163 (1988) [*ZhETF* **94**, 139 (1988)].
 - ⁵⁹ E. V. Bezuglyi, A. S. Vasenko, V. S. Shumeiko, and G. Wendin, *Phys. Rev. B* **72**, 014501 (2005); E. V. Bezuglyi, A. S. Vasenko, E. N. Bratus, V. S. Shumeiko, and G. Wendin, *ibid.* **73**, 220506(R) (2006).
 - ⁶⁰ A. A. Golubov, M. Yu. Kupriyanov, V. F. Lukichev, and A. A. Orlikovskii, *Sov. J. Microelectron.* **12**, 191 (1984) [*Mikroelektronika* **12**, 355 (1983)].